Int. J. Heat Mass Transfer. Vol. 18, pp. 775–791. Pergamon Press 1975. Printed in Great Britain

THE CALCULATION OF LOCAL FLOW PROPERTIES IN TWO-DIMENSIONAL FURNACES

E. E. KHALIL, D. B. SPALDING and J. H. WHITELAW
Imperial College of Science and Technology, Department of Mechanical Engineering, London SW7 2BX, England

(*Received* 5 *February* 1975)

Abstract—Values of local flow properties, obtained by solving appropriate conservation equations in finite-difference form and with boundary conditions corresponding to four furnace arrangements, are presented and compared with measurements.

The calculation procedure employs, a two-equation turbulence model, so that calculations can be compared with measurements of turbulence energy as well as mean-velocity components.

Calculations were performed with three combustion models, characterised by instant reaction, instant reaction with scalar fluctuations and Arrhenius reaction or eddy-break up with scalar fluctuations: comparisons with measurements obtained in the Delft, Harwell, Ijmuiden and Karlsruhe furnaces indicate that the last two lead to reasonably correct results.

NOMENCLATURE

A, pre-exponential coefficient;
a, flux-model absorption coefficient;
a_0, constant in the specific heat;
b_0, constant;
b_1, b_2, constants;
C_p, specific heat at constant pressure;
C_1, C_2, constants in turbulence model;
C_{g1}, C_{g2}, constants in combustion model;
C_D, constant;
C_R, eddy-break-up constant;
D, diameter;
E, activation energy;
E, constant of law of wall;
E_s, black body emissive power, σT^4;
f, mixture fraction, $=(\varphi-\varphi_A)/(\varphi_F-\varphi_A)$;
g, square of the fluctuation of concentration;
h, stagnation enthalpy;
H_{fu}, heat of reaction of fuel;
i, stoichiometric mass of oxygen per unit mass of fuel;
k, kinetic energy of turbulence, $=\frac{1}{2}(\bar{u}^2+\bar{v}^2+\bar{v}_\theta^2)$;
K, constant in log law;
M, molecular weight;
m, mass fraction;
P, pressure;
Q, heat flux;
R, universal gas constant;
r, radial distance from axis of symmetry;
R_o, burner outer radius;
R_f, furnace radius;
Re, Reynolds number;
R_{fu}, rate of chemical reaction;
R_ϕ, residual value;
R_x, R_y, net radiation fluxes in the x and y directions;
S, swirl number defined as: $\int WU\rho r^2\,\mathrm{d}r/(\int \rho U^2 r\,\mathrm{d}r)R_o$;
s_ϕ, source or sink term of any variable;
T, absolute temperature;
U, fluid mean velocity in the axial direction;
u, fluctuating component of axial velocity;
V, radial mean velocity;
v, fluctuating component of radial velocity;
V_θ, normal tangential velocity;
v_θ, fluctuating component of tangential velocity;
$\mathbf{V}_0$, velocity vector;
x, axial distance from burner exit;
y, radial distance from burner centre line;
y_1, distance normal to the wall;
y_a, width of burner annulus.

Greek symbols

Γ, exchange coefficient;
μ, viscosity;
ρ, density;
σ_ϕ, Schmidt and Prandtl number for any variable ϕ;
σ, Stefan–Boltzmann constant;
ε, dissipation of energy;
φ, the dependent variable $(m_{fu}-(m_{ox}/i))$;
ϕ, general dependent variable;
τ, shear stress.

Subscripts

A, air stream;
eff, effective (including the effects of turbulence);
F, fuel stream;
f, furnace;
fu, fuel;
i, species;
ox, oxidant;
pr, product;
t, turbulent;
w, wall.

1. INTRODUCTION

THE DESIGN of furnaces would be greatly facilitated by a procedure for calculating wall heat transfer and local flow properties as a function of furnace geometry and burner conditions. Such a calculation procedure would allow the influences of air/fuel ratio, mass flow rates, burner-exit geometry and enclosure dimensions on the distribution of heat flux to be determined; the regions of unburnt fuel could be located and reduced; and regions of high temperature and of consequent NO_x formation could be avoided. Design changes leading to improved performance could then be made.

The main purpose of this paper is to test one particular calculation procedure, based on the solution of conservation equations in differential time averaged form. The equations "model" the turbulent flow and the combustion processes; and so require checking by comparisons of calculated results with experimental data. Of course, experiments are also subject to uncertainty and this must be considered in the assessment.

The equations used to model the aerodynamic turbulence have been tested in several flow configurations in the past and the uncertainties which they introduce are unlikely to be as important for furnace calculations as those introduced by the combustion model. Therefore only one turbulence model is considered; but three combustion models are examined, and their results are compared with each other and with measurements.

Attempts to calculate furnace or combustion chamber performance have been reported by, among others, Pai and Lowes [1], Evans and Matthews [2], Gosman and Lockwood [3], Elghobashi and Pun [4] and Anasoulis, McDonald and Buggeln [5]. The present calculations differ from these earlier contributions in that they: (i) make use of a numerical procedure which, although used here solely in the context of two-dimensional flows, can be and has been extended to three-dimensional flows (Patanker and Spalding [6, 7]); (ii) take account of recent developments in combustion models; and (iii) include comparisons with the recent and extensive measurements of Baker, Hutchinson, Khalil and Whitelaw [8]. It should be emphasised that the turbulence model and the combustion models have been suggested previously; the turbulence model has been described by Launder and Spalding [9] and the combustion models by Spalding [10, 11].

The experimental data used for comparison purposes, in addition to those of [8], are those of: Michelfelder and Lowes [12]; Wu and Fricker [13]; and Gunther and Lenze [14]. Reference [8] is concerned with the measurement of velocity and its correlations: by contrast, [12–14] present measurements of scalar properties. Relevant details of the geometrical features of these furnaces are indicated in Section 6 where the comparison between calculations and measurements is presented. These computational experiments have been performed at a cost which is very much less than the equivalent furnace-measurement program. The validity of the calculation procedure and the three combustion models is considered in the Discussion (Section 7). The earlier parts of the paper describe the conservation equations, the physical assumptions including the turbulence and combustion models, the solution procedure and the influence of boundary conditions. A knowledge of the sensitivity of the boundary conditions is important because the designer seldom has detailed knowledge of them; indeed, the results presented in [12–14] do not provide a complete specification of boundary conditions.

2. CONSERVATION EQUATIONS AND BOUNDARY CONDITIONS

The geometry of the furnace arrangements considered here results in flows with substantial regions of recirculation and with swirl. The equations used to represent conservation of the flow properties were, therefore, elliptic in form and were expressed in cylindrical coordinates. The general form of the equation was:

$$\left[\frac{\partial}{\partial x}(\rho U\phi)+\frac{1}{r}\frac{\partial}{\partial r}r(\rho V\phi)\right] = \frac{\partial}{\partial x}\left(b\frac{\partial\phi}{\partial x}\right)+\frac{1}{r}\frac{\partial}{\partial r}\left(rb\frac{\partial\phi}{\partial r}\right)+S_\phi \quad (1)$$

with the corresponding values of b and S_ϕ indicated in Table 1.

The use of time-average equations and of the isotropic effective-viscosity hypothesis, implied by Table 1, is complemented by conservation equations for turbulent kinetic energy and dissipation rate. The advantages and limitations of the use of these equations, and a particular effective-viscosity hypothesis, are discussed in Section 3.2.

The elliptic form of the conservation equations represented by equation (1) necessitates the specification of boundary conditions, for each dependent variable, at each surface of the solution domain. This domain was a symmetrical half-section of a furnace and symmetry conditions were, therefore, imposed on the axis. The solid-wall boundary, inlet and outlet conditions corresponded to experiment wherever known: the influence of assumed boundary conditions is quantified in Section 5.

3. PHYSICAL ASSUMPTIONS

Various assumptions are implied in the equations or must be added to them. The representation of the thermodynamic properties, i.e. density, specific heat and heat of reaction are considered in the following subsection. The use of time-average equations and the present model of the turbulence are justified and explained in the second subsection. The various combustion models, the testing of which represents a major part of the contribution of the present paper, are described in the third sub-section which also contains a brief indication of the four-flux model used to represent the radiative heat transfer.

Table 1. Conservation equations corresponding to equation (1)

Conservation of	ϕ	b	S_ϕ
Mass	1	0	0
Axial momentum	U	μ_{eff}	$\frac{\partial}{\partial x}\left(\mu_{\text{eff}}\frac{\partial U}{\partial x}\right)+\frac{1}{r}\frac{\partial}{\partial r}\left(\mu_{\text{eff}} r\frac{\partial V}{\partial x}\right)-\frac{\partial P}{\partial x}$
Radial momentum	V	μ_{eff}	$\frac{\partial}{\partial x}\left(\mu_{\text{eff}}\frac{\partial U}{\partial r}\right)+\frac{1}{r}\frac{\partial}{\partial r}\left(\mu_{\text{eff}} r\frac{\partial V}{\partial r}\right)-2\mu_{\text{eff}}\frac{V}{r^2}+\frac{\rho V_\theta^2}{r}-\frac{\partial P}{\partial r}$
Tangential momentum	rV_θ	μ_{eff}	$-\frac{2}{r}\frac{\partial}{\partial r}(\mu_{\text{eff}} V_\theta r)$
Kinetic energy	k	$\frac{\mu_{\text{eff}}}{\sigma_k}$	$G_{k_1}-\rho\varepsilon$
Dissipation rate	ε	$\frac{\mu_{\text{eff}}}{\sigma_\varepsilon}$	$\frac{\varepsilon}{k}(c_1 G_{k_1}-c_2\rho\varepsilon)$
Stagnation enthalpy	h	$\frac{\mu_{\text{eff}}}{\sigma_h}$	$2a[R_x+R_y-2E]$
Mass fraction of fuel	m_i	$\frac{\mu_{\text{eff}}}{\sigma_{fu}}$	R_{fu}
Mixture fraction	f	$\frac{\mu_{\text{eff}}}{\sigma_f}$	0
Concentration fluctuation	g	$\frac{\mu_{\text{eff}}}{\sigma_g}$	$C_{g_1}G_{g_1}-C_{g_2}\rho\frac{\varepsilon}{k}g$

$$G_{k_1}=\mu_{\text{eff}}\left[2\left(\left(\frac{\partial U}{\partial x}\right)^2+\left(\frac{\partial V}{\partial r}\right)^2+\left(\frac{V}{r}\right)^2\right)+\left(\frac{\partial V_\theta}{\partial x}\right)^2+\left(r\frac{\partial}{\partial r}\left(\frac{V_\theta}{r}\right)\right)^2+\left(\frac{\partial U}{\partial r}+\frac{\partial V}{\partial x}\right)^2\right]$$

$$G_{g_1}=\mu_{\text{eff}}\left[\left(\frac{\partial f}{\partial x}\right)^2+\left(\frac{\partial f}{\partial r}\right)^2\right] \quad \text{in Model 2.}$$

$$G_{g_1}=\mu_{\text{eff}}\left[\left(\frac{m_{fu}}{\partial x}\right)^2+\left(\frac{\partial m_{fu}}{\partial r}\right)^2\right] \quad \text{in Model 3.}$$

3.1. *Thermodynamic properties*

The density of mixtures of air, the combusting gas and the combustion products can be represented with adequate precision for present purposes, by the equation of a perfect gas

$$\rho=\frac{MP}{RT} \tag{2}$$

with M and P determined with the aid of the appropriate mass fractions and Dalton's law of partial pressures.

The specific heat was calculated from the expressions

$$\bar{C}_{p_i}=a_{0_i}+b_{0_i}T \tag{3}$$

and

$$\bar{C}_{p_{\text{mix}}}=\sum_i m_i\bar{C}_{p_i}. \tag{4}$$

The definition of the stagnation enthalpy of the mixture is

$$h=m_{fu}H_{fu}+\sum m_i\bar{C}_{p_i}T+\rho[U^2+V^2+V_\theta^2]/2 \tag{5}$$

and includes the heat of reaction, H_{fu} which must be specified from a knowledge of the fuel. In the present case, single-step reactions are assumed and the values of H_{fu} for methane, and ethane (regarded as the only combusting components of the fuel) were taken from [15] and combined according to the mass fractions of the two gases in the fuel.

The constants in equations (3) and (5) are given in Table 2 and were taken from [15].

Table 2. Gas property values; constants in equations (3) and (5)

Gas	Composition	Molecular weight	$a_{0_i}\times10^{-3}$ (kJ/kg K)	$b_{0_i}\times10^{-3}$ (kJ/kg K^2)
Natural gas	CH_4–81·3%, N_2–14·4%, C_2H_6–2·9% + traces	16·04	1000	2·055
Oxygen	O_2	32·0	888·1	0·0977
Carbon dioxide	CO_2	44·0	1740·2	0·3072
Nitrogen	N_2	28·0	823·8	0·1983
Water vapour	H_2O	18·0	1002·3	0·0865

$H_{fu}=4{\cdot}07\times10^4$ kJ/kg.

3.2. *Turbulence model*

The turbulence model used for the present calculations involves the solution of the equations of conservation of turbulent kinetic energy and dissipation rate together with the definition

$$-\rho\overline{uv} = \mu_t\left(\frac{\partial U}{\partial y}+\frac{\partial V}{\partial x}\right); \quad -\rho\overline{uv}_\theta = \mu_t\left(\frac{\partial V_\theta}{\partial x}\right) \tag{6}$$

and the assumption

$$\mu_t = C_D\rho k^2/\varepsilon = \mu_{\text{eff}} - \mu. \tag{7}$$

Equation (7) implies an isotropic turbulent viscosity and, together with equation (6) and the assumed forms of the diffusion and dissipation terms contained in the equations for turbulent kinetic energy and dissipation rate, represents a limitation on the precision of the calculation of aerodynamic flow properties. It has already been shown, for example in [8], that the normal stresses vary considerably throughout the flow and these variations and any implication which they may have for the values of mean velocity will not be represented by the present model. On the other hand, the model has previously been shown to allow good predictions in a wide range of boundary-layer flows, [16, 17]; only a small amount of testing has been attempted in strongly elliptic flows, for example [4, 18]. Consequently, a purpose of this paper is to compare predictions obtained with the two-equation model with experiments and to allow the merits of the model to be appraised for use in connection with furnace–enclosure flows.

It can be expected that the turbulence model has deficiencies, but it is desirable to quantify its abilities before attempting to introduce the additional equations required by a Reynolds stress closure.

The values of the constants in the turbulence–model equations and used for the present calculations are given in Table 3 and are identical to those of [17].

Table 3. Turbulence and combustion model constants

Constant	Value
C_1	1·44
C_2	1·92
C_D	0·09
K	0·42
E	8·8
C_{g_1}	2·8
C_{g_2}	2·0
C_R	1·0

$\sigma_k = \sigma_h = \sigma_{fu} = \sigma_f = \sigma_g = 0{\cdot}9$
$\sigma_\varepsilon = K^2/[(C_2-C_1)C_D^{\frac{1}{2}}] = 1{\cdot}22$

To avoid the need for detailed calculations in the near-wall regions, equations were introduced to link the values of dependent variables on the wall to those in the logarithmic region. The wall functions (9), corresponding to the equations for the three velocity components, kinetic-energy, dissipation rate and enthalpy are:

$$\mathbf{V}_0\frac{(C_D^{\frac{1}{4}}k^{\frac{1}{2}})}{\tau_w/\rho} = \frac{1}{K}\ln[EC_D^{\frac{1}{4}}k^{\frac{1}{2}}y_1\rho/\mu] \tag{8}$$

$$k = \tau_w/\rho C_D^{\frac{1}{2}} \tag{9}$$

$$\varepsilon(y_1/k^{\frac{1}{2}}) = C_D^{\frac{3}{4}}/K \tag{10}$$

$$(T_w-T)[C_{p_{\text{mix}}}\rho C_D^{\frac{1}{4}}k^{\frac{1}{2}}/q_w] = \frac{\sigma_{h,t}}{K}\ln[EC_D^{\frac{1}{4}}k^{\frac{1}{2}}y_1\rho/\mu]+9{\cdot}24\sigma_h\left[\frac{\sigma_h}{\sigma_{h,t}}-1\right]\left[\frac{\sigma_{h,t}}{\sigma_h}\right]^{\frac{1}{4}}. \tag{11}$$

In the case of the equations for m_i, f and g, the wall values were made equal to the values at the first grid node. The values of specific heat, Prandtl number and viscosity were evaluated at the wall temperature. The values used for K and E are given in Table 3. At the symmetry axis, the gradients $\partial\phi/\partial r$ were set to zero.

3.3. *Combustion models*

Three combustion models are referred to in this paper and are described and discussed in turn.

Model 1. The first model postulates a physically controlled, one-step reaction, with fuel and oxygen unable to coexist at the same location. The only species equation to be solved is that for the mixture fraction f, this equation has no source.

Model 2. In the second model, the infinitely fast, one-step reaction is retained; but fuel and oxygen may exist at the same location, although at different times. Equations for f and for the corresponding fluctuations, i.e. g, are solved and the maximum and minimum values of f at any point, f_+ and f_-, are represented by:

$$\begin{aligned} f_+ &= f+g^{\frac{1}{2}} \\ f_- &= f-g^{\frac{1}{2}} \end{aligned} \tag{12}$$

except where the value of f_+ exceeds unity and where the value of f_- is less than zero. Equation (12) represents a symmetrical square-wave variation of f, i.e. f_+ and f_- exist for equal times; but, in regions where f_+ exceeds unity or f_- is less than zero, the factor α defined by

$$f = \alpha f_+ + (1-\alpha)f_-, \tag{13}$$

represents the proportion of time spent in the f_+ state. Values of temperature and the mass fractions of fuel and oxygen are calculated corresponding to f_+ and f_- and the mean quantities obtained from the corresponding T_+, T_-, m_{fu_+}, m_{fu_-}, m_{ox_+}, m_{ox_-} together with α. This leads, for example, to lesser values of T than would be obtained from model 1 and influences the density values used in the continuity and momentum equations. As in model 1, the f-equation has no source term but the g-equation includes a source term for generation. Further information is contained in [10, 11].

Model 3. In contrast to models 1 and 2, a finite reaction rate is introduced in model 3. It is represented by an Arrhenius-type source term or by an eddy-break up term in the fuel equation: the reaction is chosen according to which of these terms leads to the smaller rate of generation of combustion products. The Arrhenius source term may be written in the form

$$R_{fu} = m_{fu}\rho^2 m_{ox}A\exp(-E/RT) \tag{14}$$

and it can be seen that values for A and E/R are required to complete the specification: these values were assumed to be constant and equal to $10^{10}\,m^3/kgs$ and $1{\cdot}84\times10^4\,K$ respectively, in accordance with the recommendation of [19]. The eddy-break-up term may be written in the form

$$R_{fu} = C_R g^{\frac{1}{2}}(\rho\varepsilon/k). \tag{15}$$

In terms of the number of differential equations considered, model 3 requires the solution of the same equations as model 2 and in addition, the solution of an equation for m_{fu}. The equation for g has been solved but, for comparison purposes, some calculations have been performed with an explicit form of the g-equation obtained by neglecting the diffusion and convective terms. It should be noted that the source term in the g-equation is based on m_{fu} rather than on f as in the case of model 2. This is in recognition of the contribution which m_{fu} makes to the fluctuations and is allowed by the solution of the m_{fu}-equation. It should be stressed that, in proposing the use of an eddy-break-up model, Spalding [11] regarded it as a preliminary attempt to take some account of the influence of the eddy-structure of turbulence on combustion. Radiation was considered through a four-flux model incorporated in the source term of the enthalpy equation. The model is described in [20] and incorporates a flux model absorption coefficient expressed as $a = 0{\cdot}2m_{fu}+0{\cdot}1m_{pr}$.

4. SOLUTION PROCEDURE

The differential equations represented by equation (1) and Table 1 were expressed in the finite-difference form of [21] and solved by the algorithm described in the same paper. Calculations were performed with several arrangements of grid nodes and with different number of nodes: Fig. 1 displays the locations of the 20×20 nodes used for the final calculations performed in connection with the furnace geometry of [8]. The influence of node location is indicated in Section 5.

The use of a grid composed of 20×20 nodes allowed the solution of ten equations in approximately 9 min of CDC 6600 CP time: in the absence of swirl, this time reduced to approximately 4 min and in the absence of swirl and combustion to 2·5 min.

To aid the solution of the finite-difference forms of equation (1), together with the boundary conditions of Section 3.1, under-relaxation was used, in the form:

$$\phi = \beta\phi_{\text{new}} + (1-\beta)\phi_{\text{old}}. \tag{16}$$

The values of β were set to increase with the number of iterations from values of 0·3 to 0·6 for the velocity components; 0·8 to 0·9 for k and ε; and from 0·9 to 1·0 for other scalar variables.

The solutions were assumed to have converged when the maximum residual defined as

$$R_\phi \equiv \frac{[\text{convection}+\text{diffusion}+\text{source}]_{j+i}}{\phi_j}$$

was less than 10^{-4} at any grid node and for any of the ϕ equations. After thirty iterations, all calculations were observed to converge monotonically.

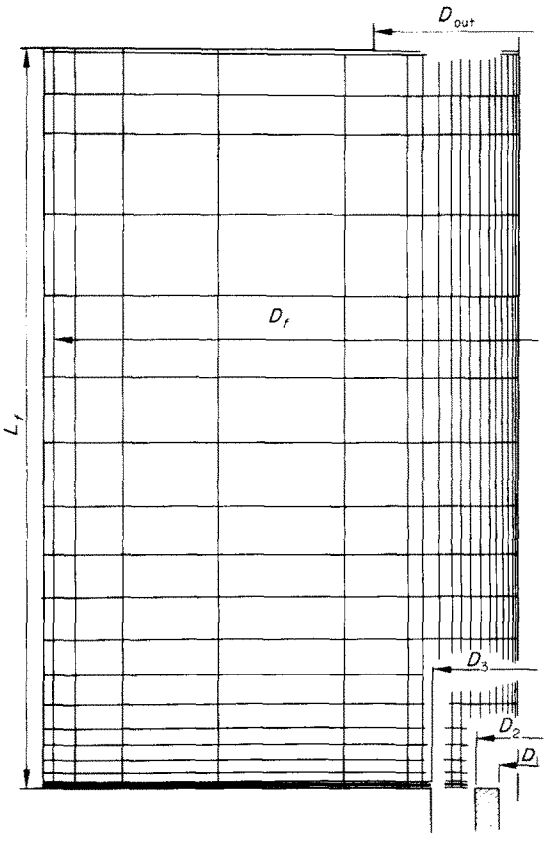

FIG. 1. Furnace and grid arrangement.

5. INFLUENCE OF INITIAL AND BOUNDARY CONDITIONS

The purpose of this section is to indicate the influence of initial and boundary conditions on calculated values of dependent variables. As indicated in Section 2, the elliptic form of the conservation equations requires that values of the dependent variables or their gradients be specified at each boundary of the solution domain. The wall functions provide this information at the solid boundaries although the value of wall temperature is required and the influence of its assumed values must be determined. In addition to the wall temperature also required are: the values of velocity, turbulent kinetic energy, dissipation rate, enthalpy, and species concentration, at the burner exit and at the exit from the furnace; these are not normally known. The influences of the assumed values are indicated here.

Figure 2 indicates the influence of the assumed shape of the velocity profile on the centre-line velocity distribution for each of three flow conditions. The mass flows and total enthalpy flux entering the furnace are the same for the upper two sets of curves and correspond to a stoichiometric condition for the combustion calculation and to the equivalent mass flow ratio for the isothermal calculation. The lower two curves correspond to the isothermal, experimental conditions of [8], i.e. the annulus mass velocity is identical to that for each of the other curves but the central jet is blocked off. The entry profiles of turbulent kinetic energy and dissipation rate were identical for each of the calculations.

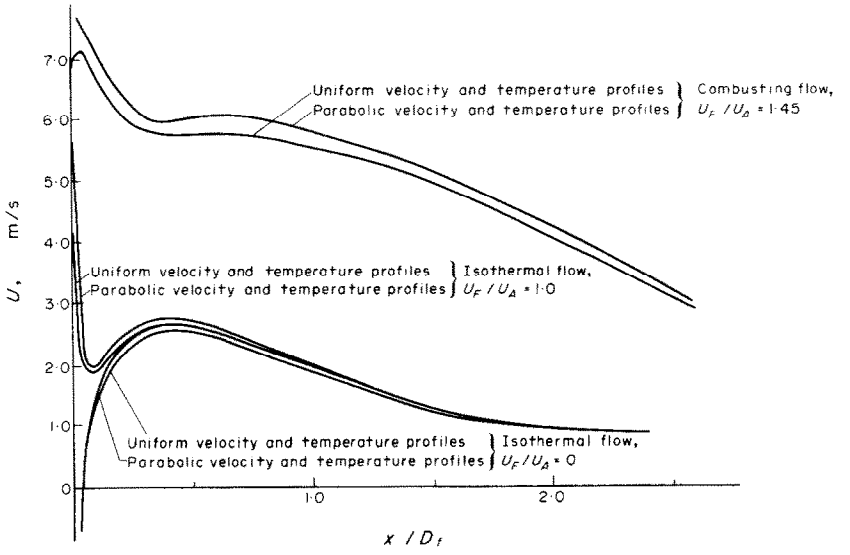

FIG. 2. Influence of initial profiles of mean velocity and temperature; swirl number = 0, isothermal and combusting flows.

The isothermal calculations show that the assumption of constant velocities in the annulus and central jet leads to downstream values of the centreline velocity which are around 2 per cent lower than those obtained with a near-parabolic profile (based on four node points). This influence was found to be considerably smaller for swirling flows. It is unlikely that, in a practical situation, the profile would be near parabolic and the influence of the initial velocity profile can therefore be neglected.

The influence of the presence of a central jet velocity can also be deduced from the lower two sets of curves and is considerable over an axial distance of six central-jet diameters. The two upper curves of Fig. 2 correspond to a combusting flow with uniform and parabolic velocity profiles for the annulus and central-core flows. The calculations show that the increase in centre-line velocity, associated with the parabolic profile, is maintained throughout the furnace although the difference appears to level off at around 0·2 m/s. This difference is reflected in the flow at locations away from the centre line. For example, in the case of the parabolic initial profiles, the recirculation zone is significantly longer and the negative velocities attain higher values. Once again, the influence was negligible for swirling flows.

Similar tests were carried out to determine the influence of the temperature distribution specified in the plane of the burner exit. It was found that, provided the total enthalpy of the incoming fluid was maintained constant, changes in the radial distribution of the fluid temperature were very small. For example, an increase in the fluid temperature of the incoming fluid from 300 to 400 K resulted in a maximum difference in fluid velocity of less than 1 per cent for downstream positions beyond three jet diameters: this influence was less in the swirling case. The temperature of the enclosure was, on the other hand, found to have a more significant influence. Tests were carried out, for the combusting flows, and demonstrated that the influence of an increase in the wall temperature of the circular enclosure from 600 to 1000 K resulted in a small increase in the dividing stream line of the recirculation zone but a more significant change in the velocity and temperature profiles: The results for the non-swirling case are shown on Fig. 3. The two sets of results shown on Fig. 3 correspond to a change in the integrated enthalpy of the flow due to the different wall temperatures: they are particularly relevant to the results of [8] where the wall temperature was not measured.

The influence of the turbulence properties, i.e. k and ε, specified in the plane of the annulus and jet exits has also been investigated. In practice, these properties are

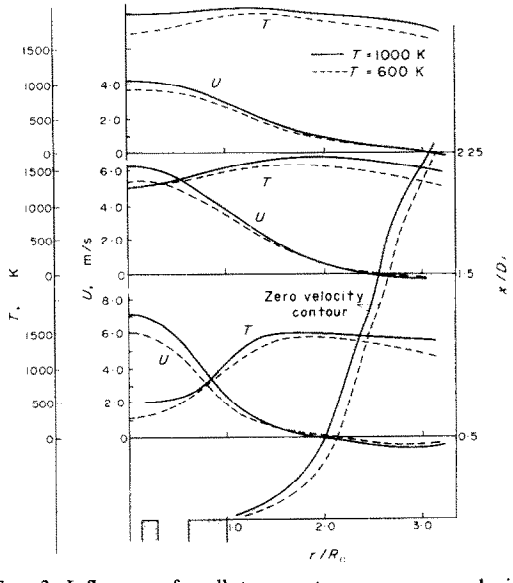

FIG. 3. Influence of wall temperature on mean velocity profiles and on the recirculation zone; swirl number = 0, combusting flow.

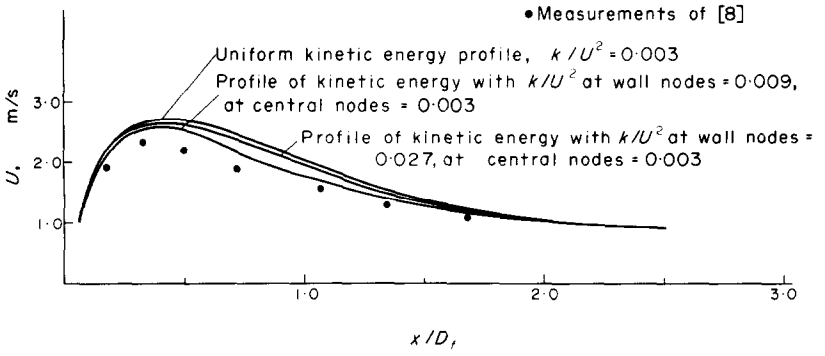

FIG. 4. Influence of initial profiles of turbulent kinetic energy and dissipation rate on mean velocity: swirl number = 0, isothermal flow.

often not known from experiment but are required by the calculation procedure as initial conditions. Figure 4 presents results for the non-swirling, isothermal flow for which the influence is greatest. These calculations were performed with a uniform distribution of mean velocity and three distributions of turbulent kinetic energy corresponding to a uniform distribution with $(\bar{u}^2)^{\frac{1}{2}}/U$ equal to 0·045 (i.e. $k/U^2 = 0{\cdot}003$); a distribution with 0·003 at the two central nodes and 0·009 ($(\bar{u}^2)^{\frac{1}{2}}/U = 0{\cdot}08$) at the two near-wall nodes; and a distribution with 0·003 at the two central nodes and 0·027 ($(\bar{u}^2)^{\frac{1}{2}}/U = 0{\cdot}135$) at the two near-wall nodes. These figures refer to the annulus flow: the central-jet velocity was zero in this case. The corresponding values of dissipation were determined from the equation:

$$\varepsilon = C_D k \frac{k^{\frac{1}{2}}}{l_{\text{mix}}} = C_D k \frac{k^{\frac{1}{2}}}{0{\cdot}03 y_a}.$$

The results show that the influence of the kinetic energy and coupled dissipation rate is appreciable and, indeed, further calculations have shown that the influence upon the centre-line mean velocity of an increase in the normalized kinetic energy from 0·003 to 0·01 at the two near-wall grid nodes is greater than a decrease in the value at the two central nodes from 0·003 to 0·0006.

Boundary conditions must be specified at the outlet from the flow and the sensitivity of these specifications was also tested for the furnace arrangement of [8]. Independent tests were carried out for U, h, f and g. In each case, calculations were compared with two specifications of the outlet conditions: in one case, the gradient $\partial\phi/\partial x$ was set to zero and in the other the gradient at the exit was set equal to that at the upstream grid node ($0{\cdot}166 D_f$ upstream of the exit plane). No significant differences in upstream calculations were observed for the four flow conditions tested, i.e. isothermal and combusting with and without swirl.

6. COMPARISON OF CALCULATIONS AND EXPERIMENTS

The calculations presented in this section are presented in a sequence which allows the reader to assess the validity of the assumptions embodied in the equations solved for aerodynamic properties, i.e. the turbulence model, and then the overall procedure embodying the turbulence model and a combustion model. In this second stage, the relative advantages of the three combustion models described in Section 3.3 will be assessed. Finally, calculations made with the preferred combustion model will be presented and appraised in order to determine the overall precision with which calculations may be performed.

The basis for the appraisal and validation indicated in the previous paragraph is largely comparison with experiments and it should be recognized that those data cannot be regarded as complete or as of known precision. Four sets of data have been selected as the basis for this comparison and were obtained in furnaces with dimensions indicated in Table 4. Those of Baker *et al.* [8] are the most complete in that they include the velocity components and corresponding normal stresses in detail and included profiles which can be used as initial values. These measurements are probably the most precise available but do not allow comparisons with those properties which are most relevant to furnace heat transfer, i.e. temperature and wall heat

Table 4. Dimensions of furnaces of [8, 12–14]

Furnace of reference	D_f (mm)	L_f (mm)	D_1 (mm)	D_2 (mm)	D_3 (mm)	D_{out} (mm)	Swirl number	Remarks
[8]	300	900	12	27	55	90	0·0 0·52	Isothermal & combusting
[14]	450	2500	10	16	81	450	0·0	Combusting
[13]	900	5000	46	60	131	270	0·0 0·84	Divergent air nozzle: combusting
[12]	2000	6000	46	60	176	900	0·0 0·5	Square cross section: combusting

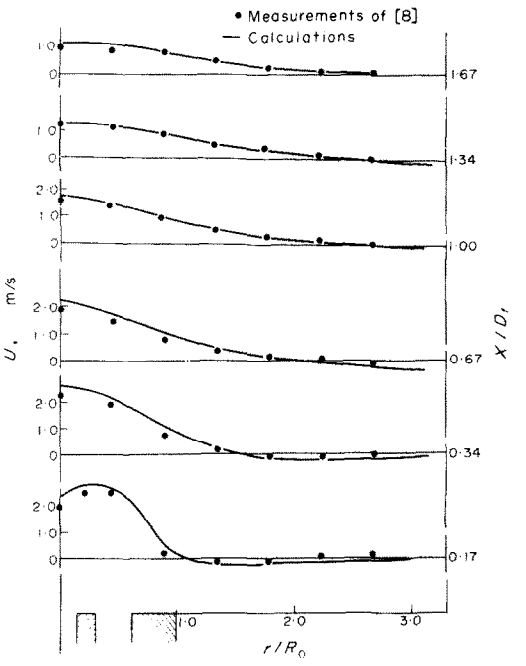

FIG. 5. Radial profiles of mean axial velocity: swirl number = 0, isothermal flow.

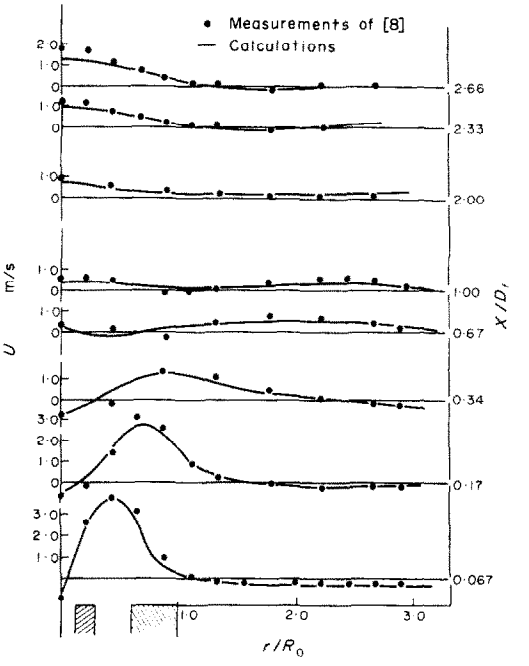

FIG. 7. Radial profiles of mean axial velocity: swirl number = 0·52, isothermal flow.

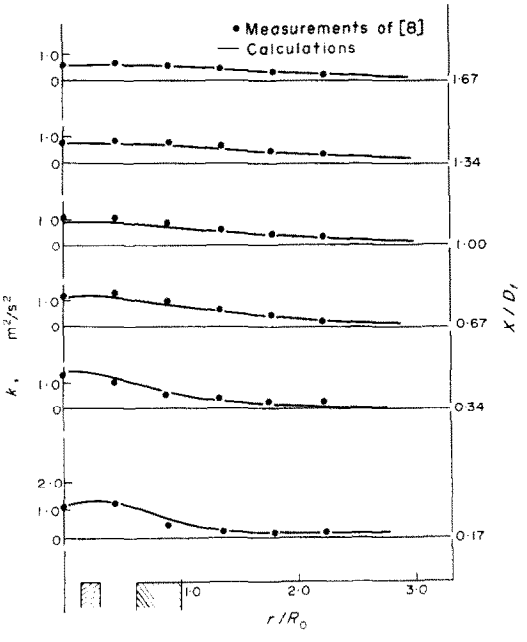

FIG. 6. Radial profiles of kinetic energy of turbulence: swirl number = 0, isothermal flow.

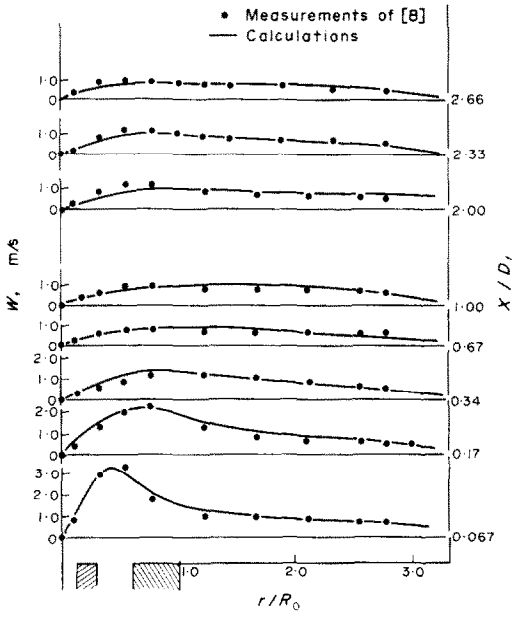

FIG. 8. Radial profiles of mean tangential velocity: swirl number = 0·52, isothermal flow.

flux. In contrast, references [12–14] relate to scalar properties and do not include detailed information of the initial values. Also, the precision of measurements is finite; further comments on this point will be made when the comparisons are presented.

6.1. *Isothermal calculations*

Calculated values of axial velocity and turbulent kinetic energy are compared with measurements on Figs. 5 and 6. The two sets of data are in good agreement with a maximum centre-line deviation of 10 per cent in the mean velocity and a maximum centre-line deviation of 15 per cent in the turbulent kinetic energy. The initial profiles corresponded as closely to the non-swirl experiments as the four grid nodes allowed with values of turbulence intensity at the near wall nodes of 0·08. There was no central jet velocity. In general, it can be said that the turbulence model provides satisfactory predictions for the non-swirling case.

The Figs. 7–9 relate to a swirling flow and compare calculated and measured values of mean-axial and circumferential velocity components and turbulent

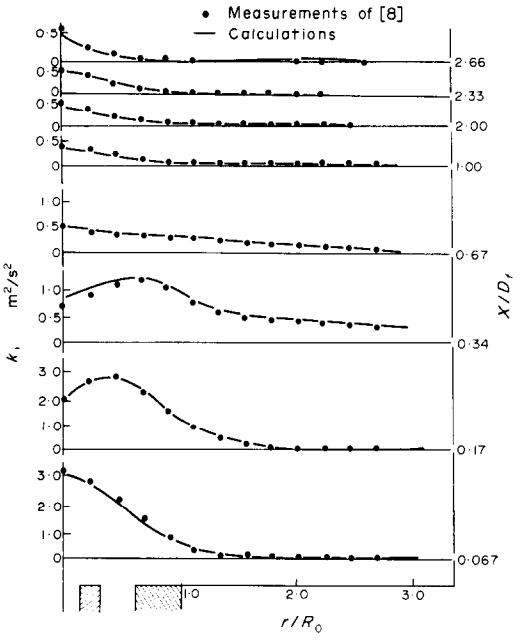

FIG. 9. Radial profiles of kinetic energy of turbulence: swirl number = 0·52, isothermal flow.

kinetic energy. The agreement is not as good as that of Figs. 5 and 6 and this may be attributed to the isotropic nature of the turbulence model. The largest discrepancy occurs in the axial mean velocity which, for example, suggests that the distribution of centre-line velocity is less well calculated in the downstream region; this may be associated with the downstream separation region where the circumferential velocity component is significantly greater than the axial component and, therefore, the probable effects of an erroneous assumption of isotropic viscosity would be most significant. Although the turbulence model appears to be less satisfactory in this swirling case, the agreement between the calculations and measurements may be regarded as satisfactory for engineering purposes: the maximum deviation between centre line calculated and measured velocities is 15 per cent.

6.2. *Combustion calculations*

6.2.1. *Comparison with velocity information and calculated temperatures.* (a) Non-swirling flame—The results presented on Figs. 10–14 correspond to the combustion measurements of [8] and indicate the extent to which the combustion models described in Section 3.3 allow realistic calculations. Figures 10 and 11 present centre-line values of mean velocity and turbulent kinetic energy obtained without swirl: corresponding distributions of mean temperature and the rms of the temperature fluctuations are presented on Fig. 12. Examination of Fig. 10 shows that there are significant differences in the magnitude of the two sets of results. In the initial region, say up to $0{\cdot}3D_f$, the discrepancy can be explained by the slight lift-off of the flame observed in the experiments: this resulted in the acceleration, due to the combustion, being delayed to a region around $D_f/6$. In contrast, the calculations indicate an initial acceleration very close to the burner followed by a decay as the lower density central jet penetrates the surrounding and burning fluid. A comparison of the calculations with the three combustion models indicates that Model 2 agrees most closely with the measurements. It is interesting to note, however, that the results obtained with model 3 are greatly influenced by the form of the g-equation: the figure includes one curve obtained with model 3 but with an algebraic solution of a form of the g-equation in which production and dissipation are assumed equal. The calculations of Fig. 11 again with the exception of the initial region, are in acceptable agreement with measurements. It is difficult to state which model is to be preferred but model 2 does again appear to be

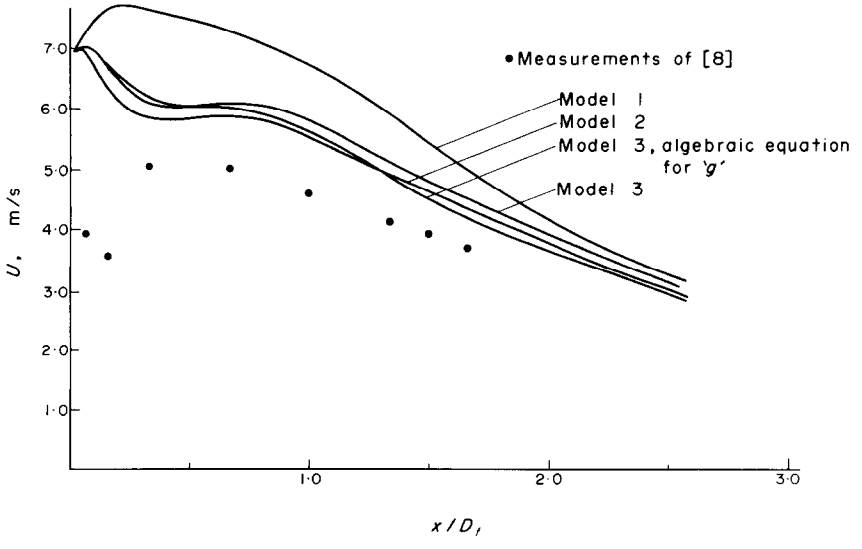

FIG. 10. Centre-line distribution of mean axial velocity: swirl number = 0, combusting flow.

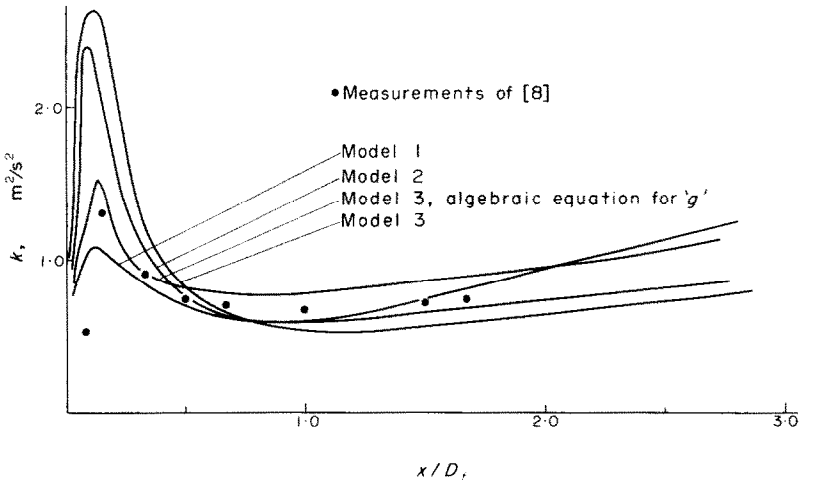

FIG. 11. Centre-line distribution of kinetic energy of turbulence: swirl number = 0, combusting flow.

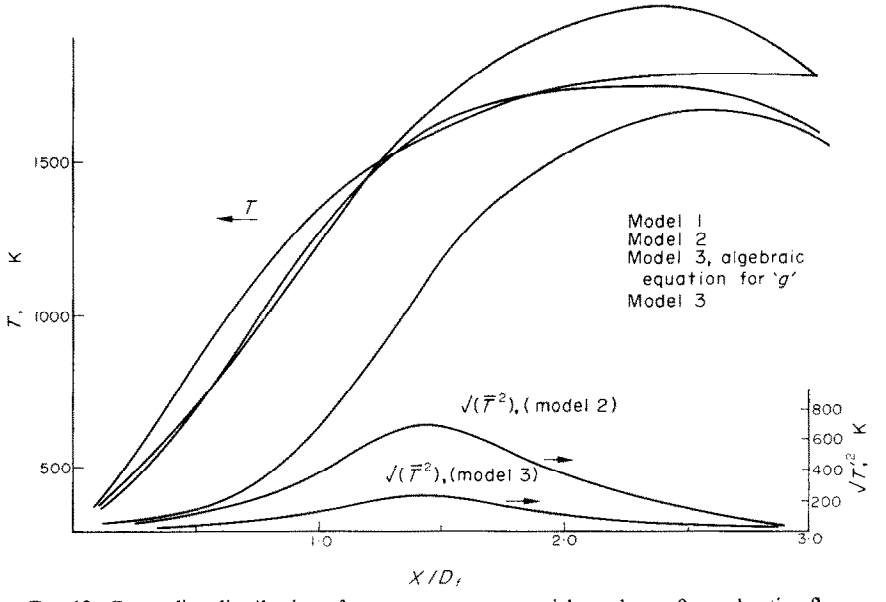

FIG. 12. Centre-line distribution of mean temperature: swirl number = 0, combusting flow.

marginally better than the others. The calculated values of mean temperature and rms of the temperature fluctuations, shown on Fig. 12, cannot be compared with experiments. The mean values indicate, however, that model 2 results in a lower maximum centre-line temperature since the maximum attainable value, the adiabatic-flame temperature, can only be attained in the case of model 1: in the other cases, the adiabatic-flame temperature will correspond to the mean value plus the fluctuation. The distributions of the RMS of the temperature fluctuations are presented in dimensional form and indicate an increase which levels off some half way along the furnace; thereafter, they decay. The shape of the distribution is significantly different from the turbulent kinetic energy distribution of Fig. 11. Comparison of the values of $(\bar{u}^2)^{\frac{1}{2}}/U$ and $(\overline{T'^2})^{\frac{1}{2}}/T$ indicates that the magnitude of the latter is very much greater than that of the former except very close to the burner and the exit. The non-dimensional temperature fluctuation attains a value of 0·95 around x/D_f of 0·4; the maximum value of $(\bar{u}^2)^{\frac{1}{2}}/U$ is around 0·25 and occurs close to the burner exit. The location of the maximum temperature fluctuation corresponds approximately to the end of the luminous zone of the flame.

The differences between the mean and RMS values of temperature obtained with models 2 and 3 are worthy of further comment. It can be seen that the sum of the mean and RMS values will result in temperature values which will be similar but with model 3 providing the larger values over the first two-thirds of the furnace. The aerodynamic patterns of the two flows are different and small differences in the values of $T+(\overline{T'^2})^{\frac{1}{2}}$ are to be expected even though the use of Arrhenius over all but the initial region of the flow might be expected to result in model 3 producing lower values. The differences in $\overline{T'^2}$ are interesting and stem from the different

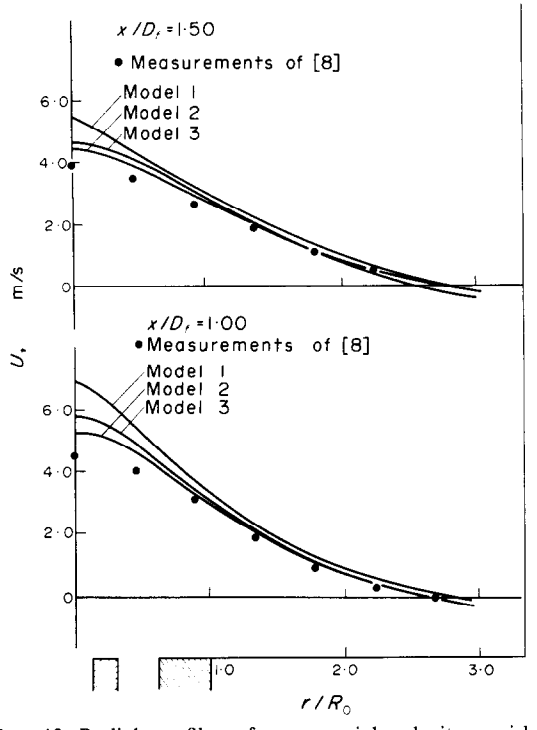

FIG. 13. Radial profiles of mean axial velocity: swirl number = 0, combusting flow.

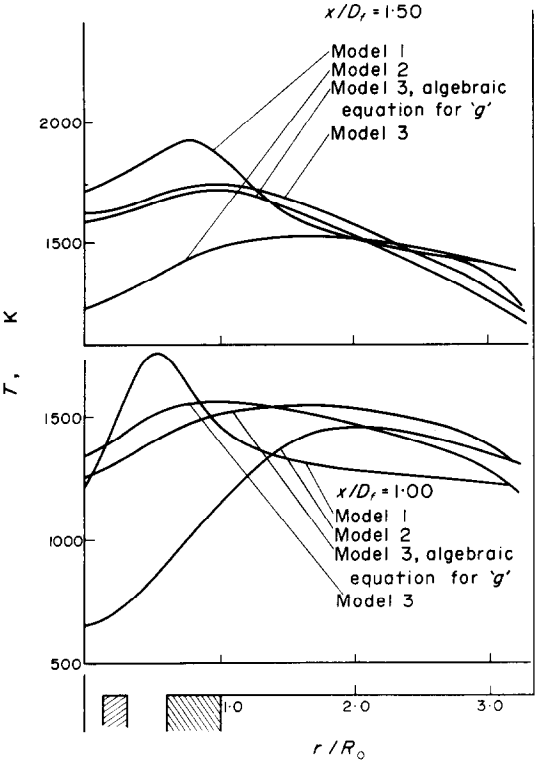

FIG. 14. Radial profiles of mean temperature: swirl number = 0, combusting flow.

source terms in the g-equations for the two models. The maximum values of $(\overline{T'^2})^{\frac{1}{2}}/T$ downstream of the immediate vicinity of the jet, achieved with models 2 and 3 are 0·64 and 0·11 respectively: measurements of Odidi [21] would suggest that the results of model 2 are closer to the truth.

Figures 13 and 14 present sample calculations of mean velocity and temperature obtained at values of x/D_f of 1·0 and 1·50. The mean velocity values may be compared with the measurements and suggest that models 2 and 3, embodying the scalar fluctuations, are to be preferred. This suggestion was supported by comparing profiles at other downstream locations, away from the initial region. The high velocity values associated with model 1 relate to the high values of mean temperature and the correspondingly low values of density used in the solution of the momentum equation for the hotter regions of the flow.

(b) *Swirling flame*—Figures 15–20 relate to the swirling measurements of [8] and present comparisons with calculations. Figure 15 presents centre-line distributions of the axial component of mean velocity and Fig. 16 the turbulent-kinetic energy. In this case, the flame was stabilized on the burner with no apparent lift off and the models should, therefore, more accurately reflect the experiments. It is clear that model 2 represents the data of both figures very well and significantly better than for the non-swirling case. The mean temperature results of Fig. 17 are similar to those of Fig. 12 although the velocity results are very different and the temperature fluctuations are only similar in general form. Thus, although in one case there is no apparent region of recirculation on the centre line and in the other region of flow recirculation exists over the upstream half of the furnace, the mean temperature distributions along the centre line are similar in shape and in magnitude. It is clear, therefore, that the radial temperature distributions must be different and this will be confirmed by results presented in the following section (Fig. 22).

The radial profiles indicated on Figs. 18–20 correspond to axial mean velocity, swirl velocity and temperature and to axial distances from the burner of 1·0 and 1·50. The calculated velocity values may be compared with measurements and again indicate that model 2 results in slightly better agreement than model 3 with model 1 a poor third. Models 2 and 3 also allow temperature calculations which are in close agreement: unfortunately there are no experiments with which to compare them.

6.2.2. *Comparison with temperature information.* The previous paragraphs allow an assessment of the merits of the present turbulence model in terms of velocity and velocity correlations but, because measured values of scalar properties were not presented in [8] any assessment of the overall calculation procedure and of the combustion model in particular is incomplete. References [12]–[14] do report temperature and wall heat flux measurements and, in an effort to improve the basis for assessment, the following six figures compare calculations with measurements. In contrast to the data of [8], however, that in [12–14] does not include adequate information of boundary conditions and reasonable assumptions have had to be made.

The furnace of Gunther and Lenze [14] has a length to diameter ratio of 5·5 but is otherwise similar to that of [8]. The centre-line distributions of mean tempera-

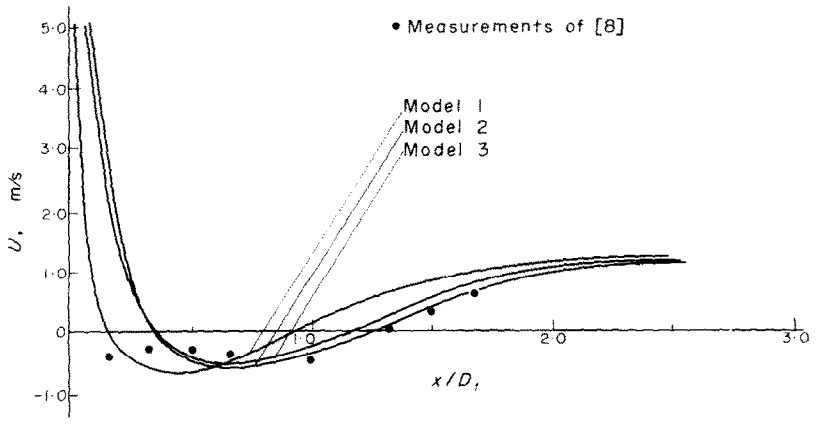

FIG. 15. Centre-line distribution of mean axial velocity: swirl number = 0·52, combusting flow.

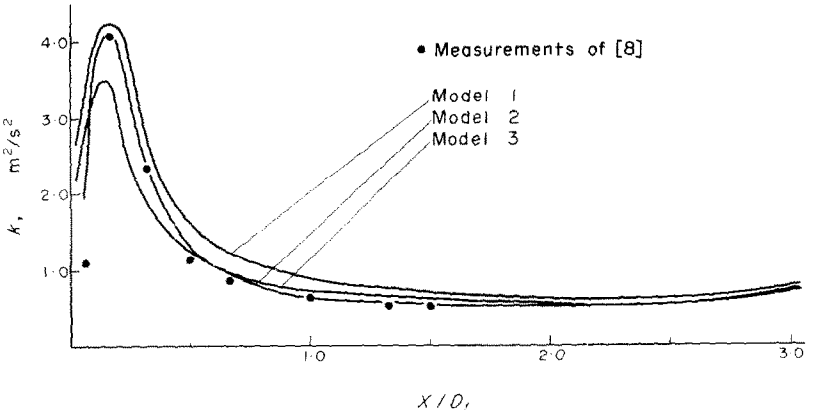

FIG. 16. Centre-line distribution of kinetic energy of turbulence: swirl number = 0·52, combusting flow.

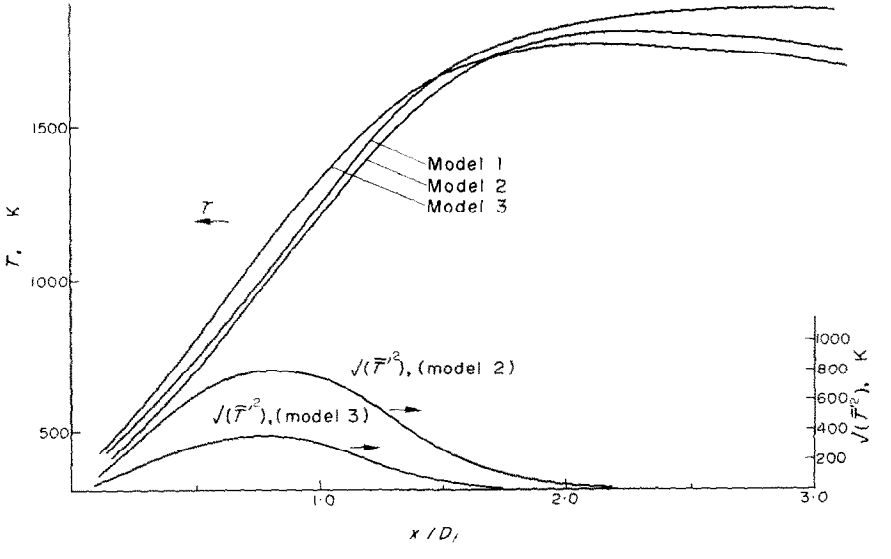

FIG. 17. Centre-line distribution of mean temperature: swirl number = 0·52, combusting flow.

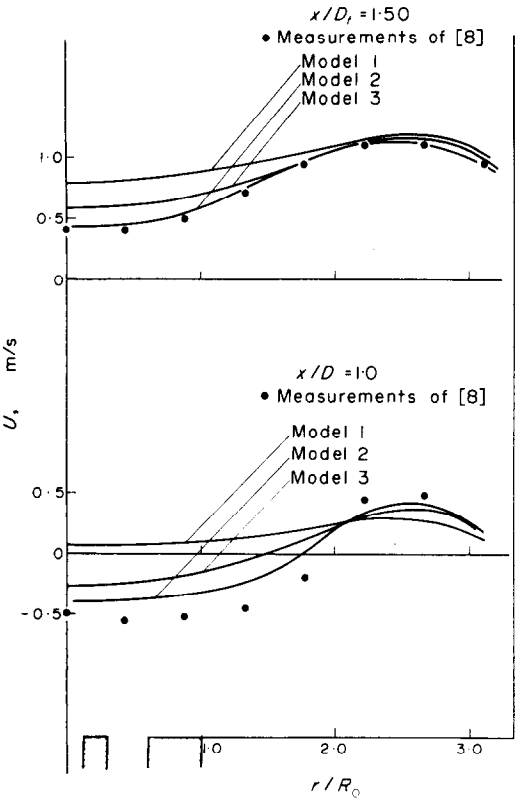

FIG. 18. Radial profiles of mean axial velocity: swirl number = 0·52, combusting flow.

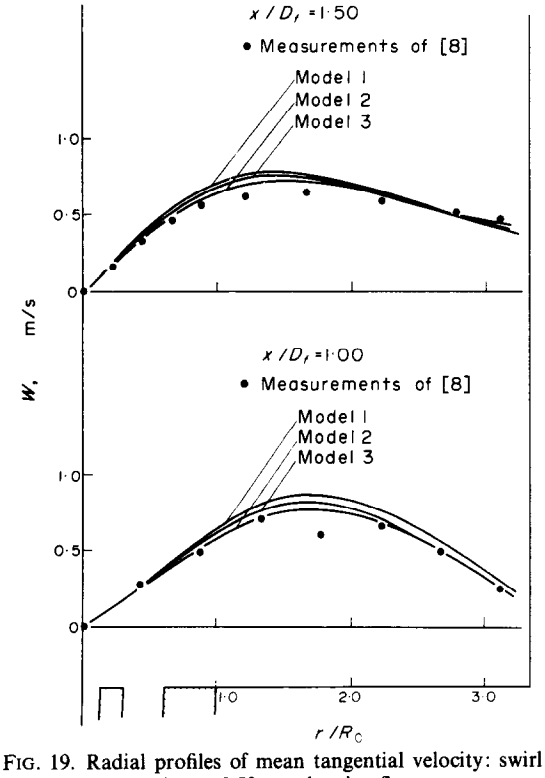

FIG. 19. Radial profiles of mean tangential velocity: swirl number = 0·52, combusting flow.

ture shown on Fig. 21 are similar to those of Fig. 12 but provide the additional information that the results obtained with model 2 are significantly lower than the measurements as well as the results of the other models.

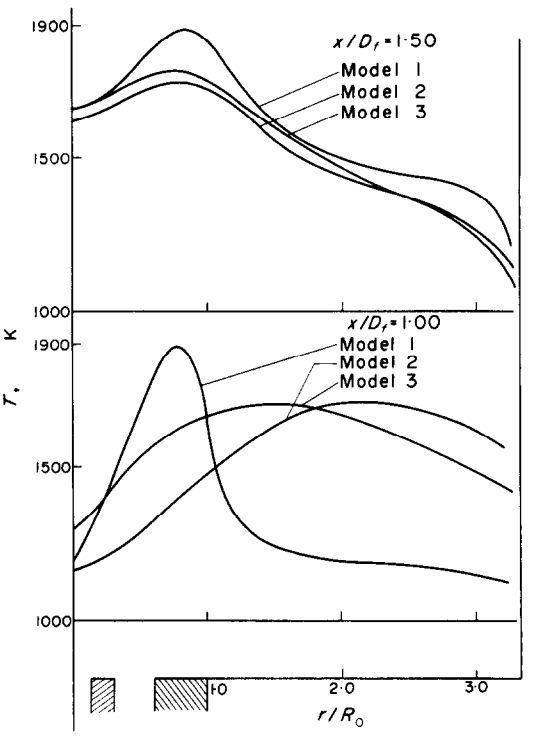

FIG. 20. Radial profiles of mean temperature: swirl number = 0·52, combusting flow.

The large difference between the temperatures calculated with model 2 and the data of models 1 and 3 stems, respectively from the consideration of temperature fluctuations and the form of the source term in the g-equation.

The additional information of Fig. 22 indicates that, although the results of models 1 and 3 were in passable agreement with experiment on the centre line they deviate considerably at other locations: the differences between the predictions obtained with the different models are again of the same magnitude as those of Fig. 14. A more complete picture of the temperature calculations is shown on Fig. 23 which compares the data provided in [14] with temperatures calculated with model 2. This figure shows that the overall pattern of the isotherms is similar but the measured flame is considerably narrower and larger than the calculated flame. The results of Figs. 4–6 suggest that the discrepancy is unlikely to stem from the turbulence model and it must, therefore, result from the combustion model or from erroneous experiments.

The furnace used for the experiments of [13] was also axisymmetric and had a length to diameter ratio of 5·17; it differed significantly from the furnaces of [8] and [14] in that the burner had a quarl exit. Figures 24 and 25 show that the results obtained with model 2 are in particularly close agreement with experiment: they also show that the predictions of the three models are in closer agreement with each other than they were on Figs. 21 and 22. This is consistent with the calculations made in connection with the results of [8] since the results of Figs. 24 and 25 correspond to a swirl number of 0·84 and those of Figs. 21–23 to a swirl number of zero.

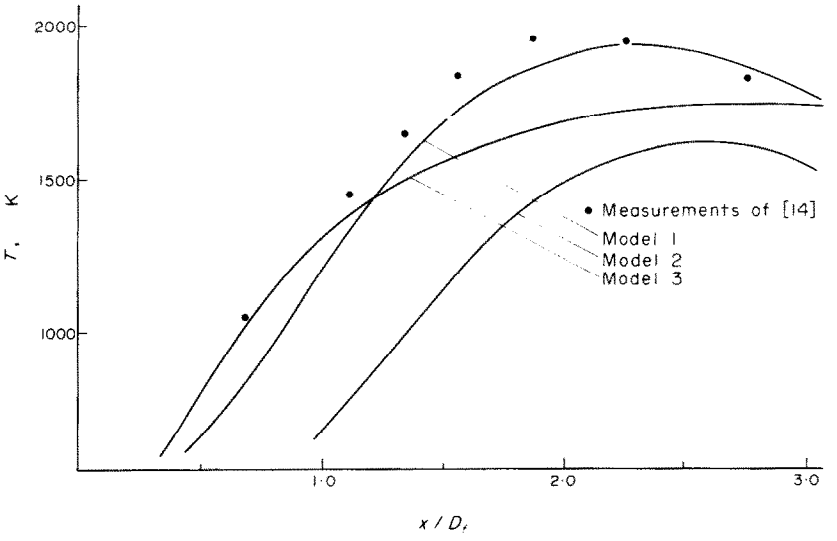

FIG. 21. Centre-line distribution of mean temperature: comparison with results of [14].

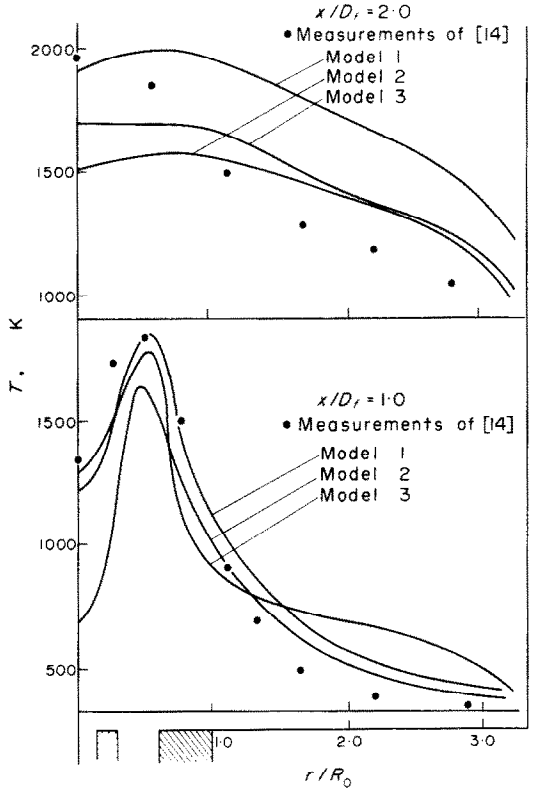

FIG. 22. Radial profiles of mean temperature: comparison with results of [14].

6.2.3. *Comparison with wall heat flux information.* Figure 26 presents values of the non-dimensional wall heat flux corresponding to the furnaces of [12] and [13]. The calculations were made using the measured distribution of wall temperature. Once again, the calculations are in agreement with the experiments for the finite swirl cases but, in general, the agreement is satisfactory for all three configurations except close to the burner and to the furnace exit: the former discrepancy could well be due to the assumed boundary conditions.

The calculated net heat flux was made up of convective and radiative components. In the case of the calculations of Fig. 26, the radiative flux was greater than the convective flux and suggests that the four flux model is a reasonable representation of the physical processes.

7. DISCUSSION AND CONCLUSION

The comparisons presented in Section 6 show that results obtained with the present procedures are in general agreement with measurements but that deficiencies still remain. The agreement is sufficient to justify calculations for many engineering purposes, although it is clear, however, that improvements can be made and the following paragraphs discuss them.

The limitations of the turbulence model can, in principle, be reduced by increasing the number of equations used to characterize the turbulence model.

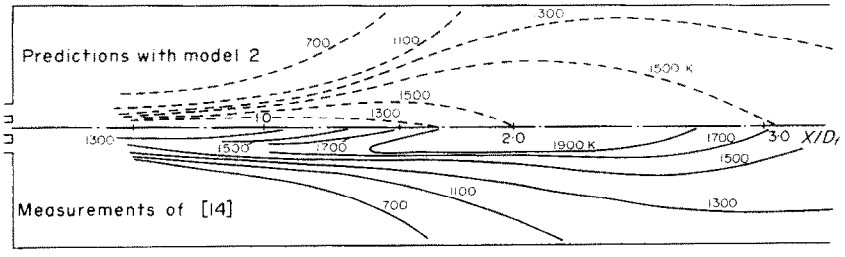

FIG. 23. Contours of isotherms; comparison with results of [14].

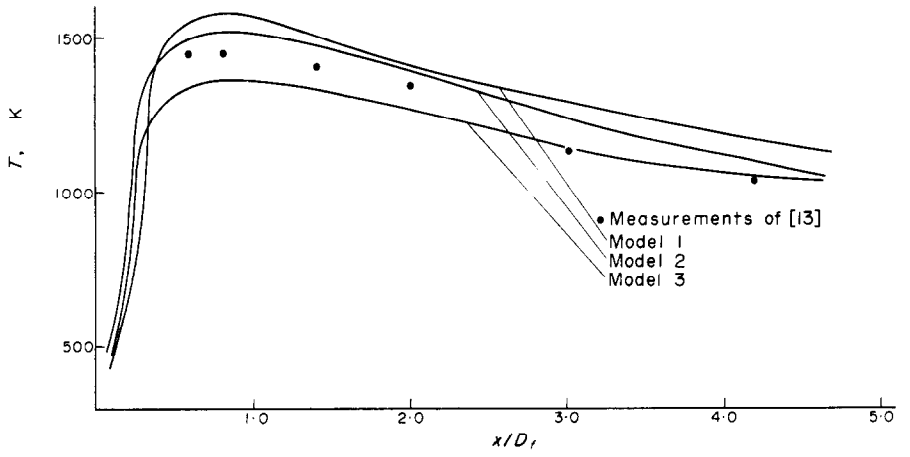

FIG. 24. Centre-line distribution of mean temperature: comparison with results of [13].

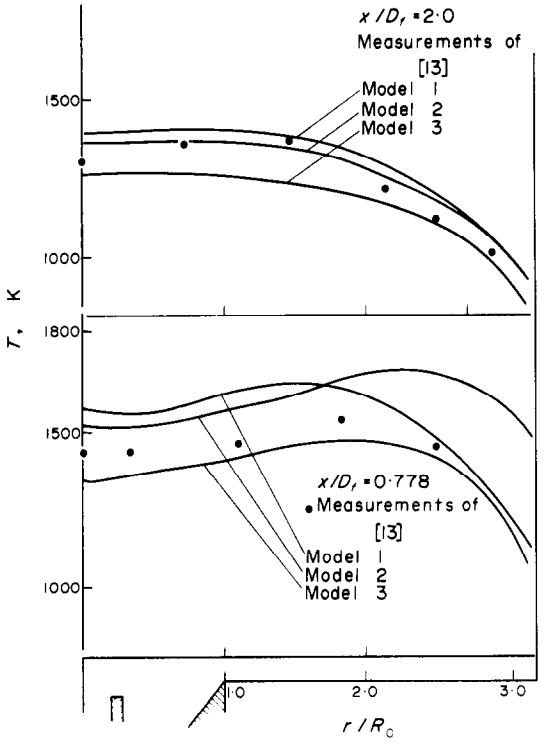

FIG. 25. Radial profiles of mean temperature: comparison with results of [13].

Equations for the normal stresses can be introduced to replace the equation for turbulent kinetic energy and additional shear stress terms represented to improve the characterization of the swirl. The present calculations indicate, that the measurements with swirl are only marginally less well calculated by the procedure and that much larger differences occur as a result of the combustion model. It seems desirable, therefore, to turn attention to the improvement of the combustion model rather than to the aerodynamic turbulence model.

A tentative conclusion which may be drawn from Section 6 is that model 2 represents the available measurements at least as well as model 3. This must result from inadequacies in the detail of model 3 rather than from the concept of recognizing finite-rate reactions. In both models 2 and 3, the square-wave form of the scalar distribution in time is the simplest possible arrangement and is a major candidate for improvement. The form of the eddy-break-up term is also in need of further consideration particularly since the eddy-break-up reaction rate controlled most of the combustion in the furnaces considered in Section 6.

The most important present need is, however, for precise measurements of velocity, temperature, species concentration and the corresponding correlations. The investigations described in [8, 12–14] are deficient for present purposes. In particular [8] does not provide

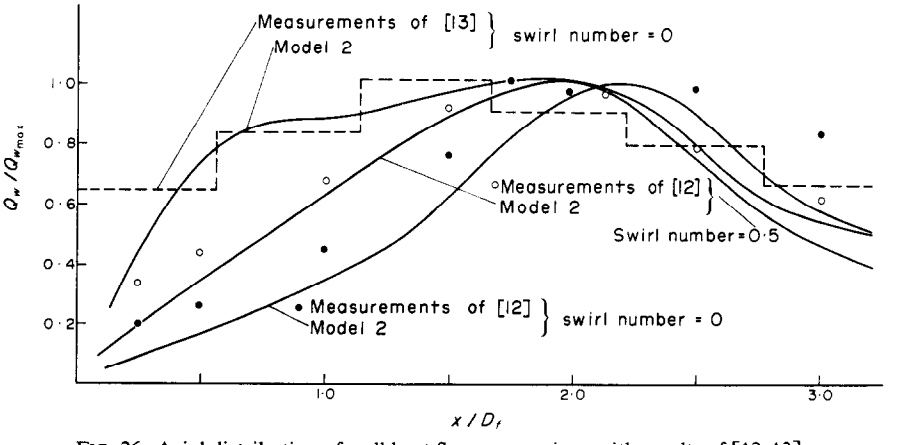

FIG. 26. Axial distribution of wall heat flux; comparison with results of [12, 13].

measurements of temperature or concentration and [12–14] provide no measurements of fluctuating properties and inadequate descriptions of the boundary conditions.

It may be concluded that the present procedure with its two-equation turbulence model, instant reaction with scalar fluctuations and four-flux radiation model is able to represent furnace flows of the type described in [8, 12–14] with a certainty which is of similar magnitude to that of the measurements. There is an immediate need for more comprehensive measurements and for the improvement of the time-fluctuation and eddy-break-up assumptions in the combustion models.

Acknowledgements—We are glad to acknowledge the technical support provided by colleagues at the AERE, Harwell and at Imperial College. Financial support was provided by the AERE, Harwell in the form of a contract to Imperial College: Dr. P. Hutchinson has monitored this contract in a constructive and helpful manner and we are particularly glad to record our appreciation and thanks to him.

The present calculations were performed with the aid of a specially adapted form of a computer program developed by Devraj Sharma for Combustion, Heat and Mass Transfer Ltd.

REFERENCES

1. B. R. Pai and T. Lowes, The prediction of flow, mixing and heat transfer in the Ijmuiden furnace, IFRF, Doc. No. 602/a/22 (1972).
2. D. G. Evans and K. J. Matthews, Computer predictions of burner fluid flow and heat release, C.E.G.B. report, R/MR 179 (1973).
3. A. D. Gosman and F. C. Lockwood, Predictions of the influence of turbulent fluctuations on flow and heat transfer in furnaces, Imperial College Mech. Eng. Dept. Report HTS/73/52 (1973).
4. S. E. Elghobashi and W. M. Pun, A theoretical and experimental study of turbulent diffusion flames in cylindrical furnaces, Proc. 15th Symposium on Combustion, see also Imperial College, Mech. Eng. Dept. Report HTS/74/16 (1974).
5. R. F. Anasoulis, H. McDonald and R. C. Buggeln, Development of a combustor flow analysis, Part 1: Theoretical studies, AFAPL–TR–73–98 (1973).
6. S. V. Patankar and D. B. Spalding, Simultaneous predictions of flow pattern and radiation for three dimensional flames, in *Heat Transfer in Flames* Edited by N. Afgan and J. Beer. Scripta, Washington, 1974.
7. S. V. Patankar and D. B. Spalding, A computer model for three-dimensional flow in furnaces, in *Proceedings 14th Symposium (International) on Combustion*, pp. 605–614. Combustion Institute, U.S.A. (1972).
8. R. J. Baker, P. Hutchinson, E. E. Khalil and J. H. Whitelaw, Measurements of three orthogonal velocity components in confined co-axial jet flows with and without swirl and combustion, Proc. 15th Symposium on Combustion. See also Imperial College, Mech. Eng. Dept. Report HTS/74/29 (1974).
9. B. E. Launder and D. B. Spalding, *Mathematical Models of Turbulence*. Academic Press, London (1972).
10. D. B. Spalding, Concentration fluctuations in a round free jet. *Chem. Engng Sci.* **26**, 95 (1971).
11. D. B. Spalding, Mixing and chemical reaction in steady confined turbulent flame, in *Proceedings 13th Symposium (International) on Combustion*. pp. 649–657, Combustion Institute, U.S.A. (1971).
12. S. Michelfelder and T. M. Lowes, Preliminary report on M–2 trials, IFRF, Doc. nr. F 36/a/4 (1972).
13. N. Fricker and H. L. Wu, An investigation of the behaviour of Swirling jet flames in a narrow cylindrical furnace, 2nd Member Conference, IFRF (1971).
14. R. Gunther and B. Lenze, Exchange coefficients and mathematical models of jet diffusion flames Proc. 14th Symposium (International) on Combustion, pp. 675–687, Combustion Institute, U.S.A. (1972).
15. S. Glasstone, *Thermodynamics for Chemists*. D. Van Nostrand, Princeton, N.J. (1946).
16. K. Hanjalic and B. E. Launder, Fully developed asymmetric flow in a plane channel. *J. Fluid Mech.* **51**, 301 (1972).
17. B. E. Launder, A. Morse, W. Rodi and D. B. Spalding, The prediction of free shear flows – a comparison of the performance of six turbulence models, NASA Conference on free shear flow, Langley field, Hampton (July 1972).
18. L. Matthews and J. H. Whitelaw, Plane-jet flow over a backward facing step. *Proc. Instn Mech. Engrs* **187**, 447 (1973).
19. V. N. Kondratiev, *Chemical Kinetics of Gas Reactions*. Pergamon Press, Oxford (1964).
20. A. D. Gosman and F. C. Lockwood, Incorporation of a flux model for radiation into a finite difference procedure for furnace calculation, Proc. 14th Symposium (International) on Combustion, pp. 661–671, Combustion Institute, U.S.A. (1972).
21. S. V. Patankar and D. B. Spalding, A calculation procedure for heat, mass and momentum transfer in three dimensional parabolic flows, *Int. J. Heat Mass Transfer* **15**, 1787 (1972).
22. A. O. Odidi, The influence of turbulence on the time-mean rate of chemical reaction, Ph.D. Thesis, University of London (1974).

CALCUL DES PROPRIETES LOCALES DE L'ECOULEMENT DANS LES FOURS BIDIMENSIONNELS

Résumé—Les valeurs des propriétés locales de l'écoulement, obtenues par résolution d'équations de conservation appropriées écrites sous forme de différences finies sont présentées et comparées aux mesures expérimentales pour plusieurs types de conditions aux limites correspondant à quatre configurations de fours.

La méthode de calcul utilise un modèle de turbulence à deux équations, si bien que les calculs peuvent être comparés aux mesures d'énergie turbulente aussi bien qu'à celles des composantes de vitesse moyenne.

Les calculs sont effectués pour trois modèles de combustion caractérisés par: une réaction instantanée, une réaction instantanée avec fluctuations scalaires et une réaction d'Arrhénius ou un émiettement des tourbillons avec fluctuations scalaires. Des comparaisons effectuées avec les mesures obtenues dans les fours de Delft, Harwell, Ijmuiden et Karlsruhe, indiquent que les deux derniers conduisent à des résultats raisonnablement corrects.

DIE BERECHNUNG DER ÖRTLICHEN STRÖMUNGSEIGENSCHAFTEN IN ZWEIDIMENSIONALEN FEUERUNGEN

Zusammenfassung—Die durch numerische Lösung der zugehörigen Bilanzgleichungen mit vier verschiedenen Feuerungsanordnungen und entsprechenden Randbedingungen gewonnenen Werte der örtlichen Strömungseigenschaften wurden mit denen aus Messungen verglichen. Die Berechnungsmethode verwendet ein Zwei-Gleichungs-Turbulenzmodell, so daß die Berechnungen mit Messungen sowohl der Turbulenzenergie als auch Komponenten der mittleren Geschwindigkeiten verglichen werden können. Die Berechnungen wurden mit drei Modellen der Verbrennung durchgeführt, die charakterisiert sind durch sofortige Reaktion, sofortige Reaktion mit skalaren Fluktuationen und Arrhenius-Reaktion oder Wirbelauflösung mit skalaren Fluktuationen. Vergleiche mit Messungen aus Feuerungen in Delft, Harwell, Ijmuiden und Karlsruhe zeigen, daß die beiden letzten Modelle zu ausreichend genauen Ergebnissen führen.

РАСЧЕТ ЛОКАЛЬНЫХ ХАРАКТЕРИСТИК ТЕЧЕНИЯ В ПЛОСКИХ ПЕЧАХ

Аннотация — Приводятся значения локальных характеристик течения, полученные путем решения соответствующих уравнений сохранения в конечных разностях при граничных условиях, соответствующих печам четырех конструкций. Полученные значения сравниваются с результатами измерений.

При расчете используется математическая модель турбулентности, представленная двумя уравнениями, так что сравнение расчетных данных с результатами эксперимента производится по энергии турбулентности и составляющим средней скорости.

Расчеты проводились на трех моделях процесса горения, характеризуемых мгновенной реакцией, мгновенной реакцией с флуктуациями скалярных величин и реакцией Аррениуса с флуктуациями скалярных величин. Сравнение численных данных с результатами измерений, полученными для печей исследователями в Дельфте, Харуэлле, Ймюдене и Карлсруэ показывает хорошее совпадение для двух последних случаев.